Original article

Patient-specific *in silico* prediction of outcomes of partial continuous-flow LVAD treatment in peripartum cardiomyopathy

Juliet Nagawa[1]*, Kevin L. Sack[1,2], N. John Nchejane[1], Y. Dodzi Motchon[1], Mazin S. Sirry[1,3], Sarah Kraus[4,5], Neil H. Davies[6], Ntobeko A.B. Ntusi[4,5,7], Thomas Franz[1,8]*

[1]Biomedical Engineering Research Centre, Division of Biomedical Engineering, Department of Human Biology, Faculty of Health Sciences, University of Cape Town, Observatory, South Africa

[2]Cardiac Rhythm Management, Medtronic Inc, Minnesota, USA

[3]Department of Biomedical Engineering, College of Engineering and Computing, International University Kuwait, Ardiya, Kuwait

[4]Department of Medicine, Faculty of Health Sciences, University of Cape Town, Observatory, South Africa

[5]Cape Heart Institute, Faculty of Health Sciences, University of Cape Town, South Africa

[6]Cardiovascular Research Unit, Faculty of Health Sciences, University of Cape Town, Observatory, South Africa

[7]SAMRC/UCT Intersection of Noncommunicable Diseases and Infectious Diseases Unit, Faculty of Health Sciences, University of Cape Town, Observatory, South Africa

[8]Bioengineering Science Research Group, Department of Mechanical Engineering, Faculty of Engineering and Physical Sciences, University of Southampton, Southampton, United Kingdom

Running title: Patient-specific prediction of outcomes of LVAD treatment in PPCM

*Corresponding authors: Juliet.Nagawa@uct.ac.za, Thomas.Franz@uct.ac.za

ORCIDs

J Nagawa: 0000-0002-3712-9647

KL Sack: 0000-0002-8253-1504

NJ Nchejane: 0000-0003-3983-7476

YD Motchon: 0000-0002-6222-3483

MS Sirry: 0000-0003-3735-0963

S Kraus: 0000-0002-4754-2953

NH Davies: 0000-0003-0432-4515

NBA Ntusi: 0000-0003-2347-7883

T Franz: 0000-0002-1504-3842

Abstract

Patients with severe peripartum cardiomyopathy (PPCM) often receive mechanical circulatory support with good outcomes. However, mechanisms underlying the functional improvements are poorly understood for patients with different PPCM characteristics. This study investigated effects of partial, continuous-flow left ventricular assist device (LVAD) support on cardiac function and mechanics in patients with different PPCM severity. Patient-specific biventricular finite element models of six patients with different PPCM severity were developed from magnetic resonance images and combined with a circulatory system model, including variable LVAD support. Ventricular function and myocardial mechanics were predicted and changes due to LVAD support were quantified. The LVAD support decreased LV myofiber stress and increased ejection fraction (EF). EF increased steadily (two patients), fluctuated (two patients), or peaked before a steady decrease (two patients) with increasing LVAD speed. Improvement due to LVAD support was greater for PPCM patients with higher disease severity than those with lower disease severity. The LVAD and native LV jointly generated stroke volume (SV) in four patients, and the LV contribution diminished with increasing LVAD speed. In the two patients with the lowest EF, the LVAD was the sole source of SV. The improvement of cardiac function and mechanics due to LVAD support in PPCM exceeds that reported for chronic heart failure due to ischemia. However, the predicted variability of the LVAD benefits with PPCM severity and mechanical support level suggests the need and potential for further studies to guide clinicians in selecting personalised treatment parameters required for optimised LVAD therapy for each PPCM patient.

Keywords: Cardiac mechanics, ventricular function, finite element modelling, biventricular geometry, mechanical circulatory support, left ventricular assist device.

Abbreviations

cMRI	Cardiac magnetic resonance imaging
ED	End-diastole, end-diastolic
EDV	End-diastolic volume
EF	Ejection fraction
ES	End-systole, end-systolic
FE	Finite element
IQR	Inter-quartile range
LV	Left ventricle, left ventricular
LVAD	Left ventricular assist device
LVEF	Left ventricular ejection fraction
LVLS	Left ventricular long-axis shortening
PPCM	Peripartum cardiomyopathy
PCWP	Pulmonary capillary wedge pressure
rpm	Revolutions per minute
RV	Right ventricle, right ventricular
RVEF	Right ventricular ejection fraction
SV	Stroke volume

1. Introduction

Cardiomyopathies ranked as the second leading cause of heart failure in Sub-Saharan Africa, with Southern Africa exhibiting the highest prevalence (40%) of cardiomyopathies, according to Agbor [1]. Moreover, peripartum cardiomyopathy (PPCM) was among the most common cardiomyopathies in Sub-Saharan Africa [1]. In South Africa, PPCM is the largest contributor to maternal death [2, 3]. In addition, studies have shown that women of African ethnicity have a higher risk of developing PPCM and obtaining poorer outcomes than women of other ethnicities [4, 5]. Moreover, poorer maternal and neonatal outcomes often present in African countries with poor socioeconomic characteristics [6].

Therapy efficacy for PPCM has mixed outcomes. While many patients respond positively to treatment, some never recover, and others die despite optimal therapy [7, 8]. PPCM is associated with high recovery rates compared to other cardiomyopathies and about 59% of PPCM patients have recovery of LV function while 1 in 10 PPCM patients die with in the first year of diagnosis [8, 9]. In cases of severe PPCM, the left ventricular assist devices (LVAD) have been used among other mechanical circulatory support therapies such as the biventricular assist device, peripheral veno-arterial extracorporeal membrane oxygenation pump, and the total artificial heart [10].

These therapies have achieved remarkable left ventricular (LV) recovery and high survival rates for PPCM patients [11, 12]. For instance, Berliner [11] reported that LVAD treatment resulted in a high recovery rate of 25% with successful LVAD explantation and a high survival rate of 91.7%. Djordjevic [13] reported a ventricular recovery rate of 20% and a survival rate of 87%. However, the mechanisms associated with the reported positive outcomes of device therapy in PPCM are poorly understood and it is not yet clear how patient-specific characteristics influence outcomes of the LVAD support.

Due to their high costs, circulatory support devices including LVADs have been administered primarily in developed countries, whereas their use has been limited in Africa [2] despite generally higher PPCM incidence (e.g. Nigeria 98:10,000 live births [14], South Africa 10:10,000 [15] than in developed countries except the USA with high proportion of people with African ethnicity (e.g. USA 11.8:10,000 [16], Germany 6.7:10,000 [17], Japan 0.5:10,000 [18]. Moreover, causes and outcomes of heart failure in Africa are different compared to high-income countries; African patients present at a younger age and exhibit higher mortality rates [19, 20]. It is therefore important to investigate outcomes of the LVAD for African patients.

The Heart Failure Society of South Africa recently developed guidelines for the effective use of LVADs in low-resource settings [21]. Rapid technological advancements and increasing emphasis on affordable healthcare solutions are expected to decrease the costs of healthcare technology in the near future. In this context, a better understanding of the therapeutic effects of LVAD support in PPCM can lead to considerable improvements to the treatment of these patients and adapted for other heart failure patients in Africa.

In silico studies can contribute to gaining knowledge on cardiac mechanics and the effects of circulatory support devices for PPCM patients with different disease severity. Finite element models have been used to investigate cardiac disease and therapeutic mechanisms for heart failure. These models enable the modification and analysis of therapeutic and disease parameters that may not be possible in experimental studies due to ethical considerations. For example, such studies have provided insights into biomechanical mechanisms of heart failure and myocardial infarction and the development and efficacy evaluation of therapies involving LVADs [22, 23], biomaterial injections [24, 25], valve repair [26] and surgical restoration [27].

In addition, the rapid increase in demand for personalised medicine and the advancement of technology has encouraged the use of patient-specific computation models to quantify effects of heart failure therapies on cardiac function, mechanics and remodelling during heart failure, which is not easily achieved with other methods [28].

The current study aimed to investigate how disease severity affects the efficacy of partial LVAD support in South African PPCM patients using patient-specific finite element models.

2. Methods

2.1. Ethical Approval

The protocol and procedures for the current study were approved by the Faculty of Health Sciences Human Research Ethics Committee of the University of Cape Town (HREC REF: 752/2018). The study conformed with the standards set by the latest version of the Declaration of Helsinki, except for registration in a database. This study only involved the use existing observational data from the IMHOTEP clinical registry of cardiomyopathy patients, and no experiments were conducted on human participants. Data collection for the IMHOTEP registry was also approved by the Faculty of Health Sciences Human Research Ethics Committee of the University of Cape Town (HREC 766/2014) and data was only collected from participants who provided written informed consent, including for data reuse in different research studies beyond the life and specific remit of the ethics approval, such as the current study. The identification of patients has been anonymised.

2.2. Patient data

The definition of PPCM by Sliwa [29] was used as inclusion criteria, and patients who did not fit this definition were not considered in the current study. Six female patients with PPCM with an age range from 19 – 41 years were included in the current study.

In vivo cardiac magnetic resonance imaging (cMRI) and echocardiographic data for six adult PPCM patients were obtained from existing records at Groote Schuur Hospital. A longitudinal dataset was used and information of the patient's diagnosis at baseline and recovery status after treatment was available from the clinical records at the beginning of this study. Recovery implied that the patient's cardiac function normalised after treatment whereas non-recovery implied that the patient's cardiac function did not normalise after treatment. A pseudonym was used for each patient representing LV ejection fraction (EF) after diagnosis at baseline, recovery status (R: recovered, N: not recovered), and survival status (A: alive, D: died) from existing records at the beginning of this study: R45A, N39A, R20A, N18A, N12A and N06D. Four patients had severely abnormal LV function with EF < 30% based on the recommendations of the American Society of Echocardiography and the European Association of Cardiovascular Imaging [30, 31]. One patient (N39A) had LV concentric remodelling (normal LV mass ≤ 95 g/m^2 with increased relative wall thickness > 0.42) whereas the other five patients had normal LV geometries as defined by Lang [30], see Table 1.

Table 1: Clinical *in vivo* cardiac metrics for the left ventricle (LV) and right ventricle (RV) of PPCM patients (PCWP: Pulmonary capillary wedge pressure, RWT: Relative wall thickness).

Patient	**LV Mass (g/m^2)**	**LV RWT**	**LV PCWP (mmHg)**
R45A	76	0.29	12
N39A	69	0.45	23
R20A	89	0.23	14
N18A	74	0.21	22
N12A	71	0.24	16
N06D	68	0.37	23

2.3. Development of cardiac geometries

Three-dimensional biventricular cardiac geometries truncated at the base were reconstructed from short-axis cMRI data at early diastole to approximate the unloaded *in vivo* configuration (Simpleware ScanIP, Synopsys, Mountain View, CA, USA). The geometries were meshed using approximately 85,000 quadratic tetrahedral elements (Figure 1 a), i.e. 85,078 for R45A, 85,656 for N39A, 85,075 for R20A, 85,321 for N18A, 85,040 for N12A, and 85,026 for N06D, following a mesh convergence study. The mesh sizes allowed adequate element distribution across the ventricular wall thickness essential for accurate fibre representation and determination of stress and strain. Similar findings were reported in a mesh convergence study by Sack [32].

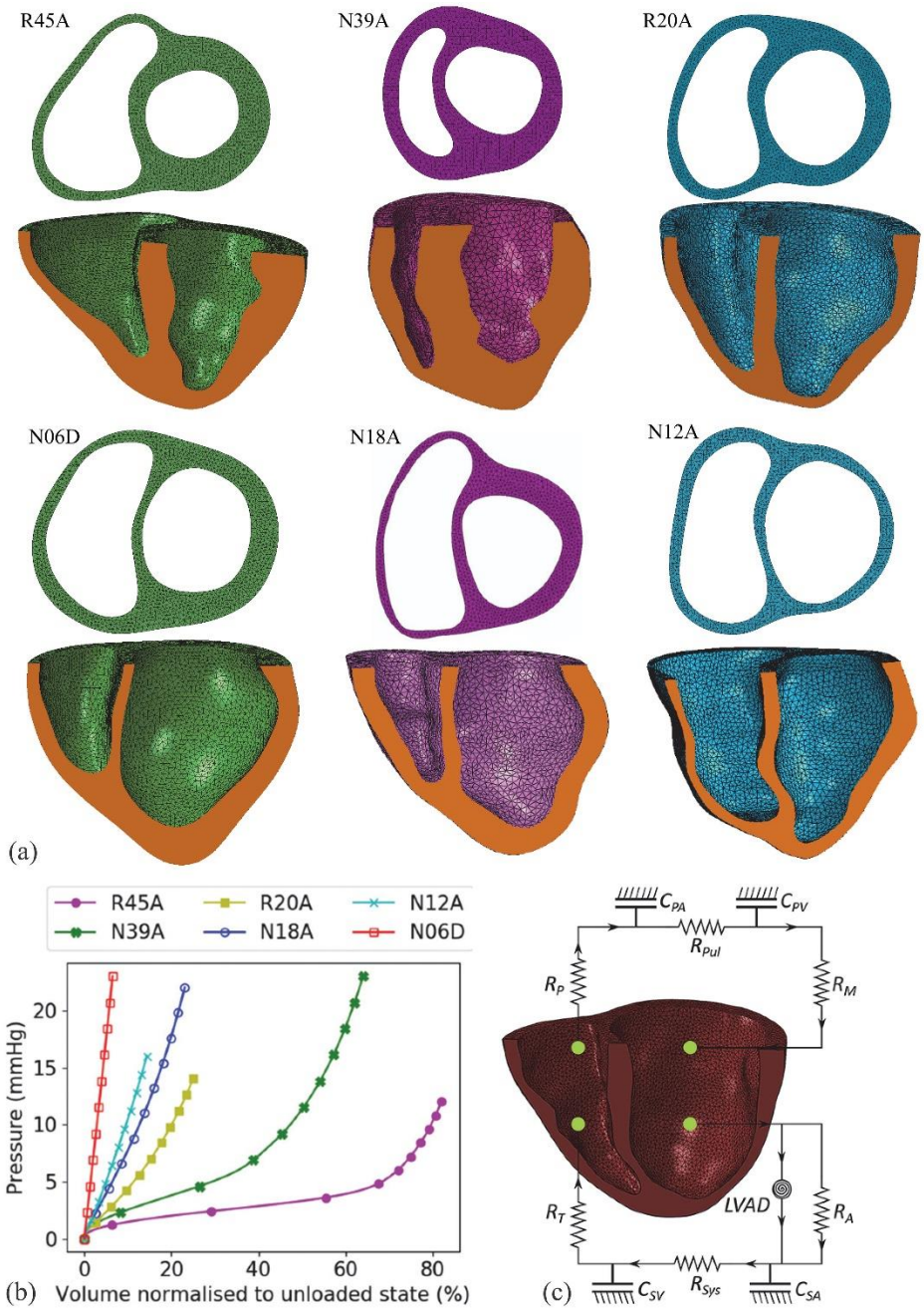

Figure 1: a) Short- and long-axis views of biventricular meshed geometries of six PPCM patients illustrating the wall thickness of the left and right ventricular free wall and septal wall. In each image, the LV is on the right, and the RV is on the left. Ejection fraction is indicated by the number in the patient code. b) Comparison of the calibrated passive filling curves for each patient. Volume was normalised to unloaded volume V_0. Compliance of the LV myocardium increased with increase in ejection fraction (numerical value in the model's name). Model N06D with the lowest ejection fraction of 6% had the stiffest LV myocardium. c) Schematic of coupling of biventricular geometry with circulatory system and LVAD [22]. R_M: mitral valve resistance, R_A: aortic valve resistance, C_{SA}: systemic arterial compliance, R_{SYS}: systemic arterial resistance, C_{SV}: systemic venous compliance, $R_{T:}$ tricuspid valve resistance, R_P: pulmonary valve resistance, C_{PA}: pulmonary arterial compliance, R_P: pulmonary valve resistance, C_{PV}: pulmonary venous compliance, LVAD: left ventricular assist device.

2.4. Development of cardiac finite element models

The meshed biventricular cardiac geometries were imported into Abaqus CAE (Dassault Systèmes, Providence, USA).

2.4.1. Boundary conditions

The LV and RV cavities were closed with caps created using two-dimensional triangular surface elements between basal endocardial nodes and central cavity nodes (one for the LV and three for the RV). The cavity caps facilitated the calculation of cavity volumes to assess ventricular function. The endocardial and central nodes at the base were fixed in the cardiac longitudinal direction to prevent rigid body motion of the biventricular geometry. The degrees of freedom of the central nodes were coupled to the average motion of the endocardial nodes, allowing movement of the endocardial and epicardial nodes at the base in the short-axis plane.

2.4.2. Myofibre orientation

Using a rule-based method, the myofibre orientation was implemented as a linear variation of the helix angle from -60º on the epicardium to +60º on the endocardium in all elements, except those forming the cavity caps, using a custom MATLAB script (The MathWorks, Inc., Natick, Massachusetts, United States) [22]. The LV and RV free walls and the septal wall had the same myofiber description [22].

2.4.3. Constitutive law for myocardium

The description of material properties of the myocardium was based on Sack [32]. The passive material properties were defined with an anisotropic hyper-elastic formulation [33]. The strain energy potentials Ψ_{iso} and Ψ_{vol} govern the isochoric and volumetric responses, respectively, and capture the experimentally observed exponential and anisotropic elastic response and near-compressibility [34]:

$$\Psi_{iso} = \frac{a}{2b} e^{b(I_1 - 3)} + \sum_{i=f,s} \frac{a_i}{2b_i} \left\{ e^{b_i (I_{4i} - 1)^2} - 1 \right\} + \frac{a_{fs}}{2b_{fs}} \left\{ e^{b_{fs} (I_{8fs})^2} - 1 \right\}, \tag{1}$$

$$\Psi_{vol} = \frac{1}{D} \left(\frac{J^2 - 1}{2} - \ln(J) \right). \tag{2}$$

All parameters are described in Table 2. The active material law is based on a time-varying elastance model by Guccione [35] and a more detailed description can be found in Sack [22]. The active tension T_a is:

$$T_a(t, l) = T_{max} \cdot \frac{Ca_0^2}{Ca_0^2 + ECa_{50}^2(l)} \cdot \frac{\left(1 - \cos\left(\omega(t, E_{ff})\right)\right)}{2}. \tag{3}$$

The maximum active tension T_{max} is multiplied by two terms governing the calcium concentration and the time of contraction, respectively. The formulation of the active tension considers sarcomere length l, which affects the stress components in the fibre direction and captures the Frank-Starling effect [36]. The total stress in the fibre direction, σ_f, and sheet direction, σ_s, are:

$$\sigma_f = \sigma_{pf} + \sigma_{af} \tag{4}$$

$$\sigma_s = \sigma_{ps} + n_s\sigma_{af} \tag{5}$$

where σ_{pf} is the passive stress in fibre direction, σ_{af} is the active stress in fibre direction, and σ_{ps} is the passive stress in sheet direction. A fraction of the active stress in fibre direction that is transferred to the sheet direction was accounted for by a scalar $n_s \epsilon$ (0,1) [22, 32].

Table 2: Constitutive parameters for the passive and active material response of the myocardium [32].

Parameter	Description
a, b	Scales isotropic tissue response
a_f, b_f	Scales additional stiffness in fibre direction
a_s, b_s	Scales additional stiffness in sheet direction
a_{fs}, b_{fs}	Scales coupling stiffness in fibre and sheet directions
A_i	Vector in direction i
I_1	First deviatoric strain invariant
I_{4i}	Pseudo-invariant defined as $A_i \cdot C \cdot A_i$
I_{8fs}	Pseudo-invariant defined as $A_f \cdot C \cdot A_s$
C	Right Cauchy-Green tensor
D	Multiple of bulk modulus ($K = 2/D$)
J	Third deformation gradient invariant
t_0	Time to reach peak tension
m	Governs slope of relaxation
b	Governs length of relaxation
l_0	Sarcomere length below which no active force develops
B	Governs shape of peak isometric tension-sarcomere length relation
Ca_0	Peak intercellular calcium concentration
Ca_{max}	Maximum intercellular calcium concentration
T_{max}	Contractility scaling factor (value directly scales ejection fraction)
E_{ff}	Lagrangian tensor component aligned with local muscle fiber direction
n_s	Fraction of active tension to be applied in sheet direction
n_n	Fraction of active tension to be applied in sheet-normal direction
l_r	Initial sarcomere length

2.5. Patient-specific optimisation of myocardial constitutive parameters

2.5.1. Passive mechanical properties

To obtain patient-specific passive material parameters, the linear (a_i) and exponential (b_i) terms, in Eqn. (1) were optimised by minimising the error between the LV end-diastolic pressure values predicted by

the FE model and those obtained from the patient's Klotz curve [37]. The LV end-diastolic pressure and volume values were used in the method described by Klotz [37] to estimate each patient's LV end-diastolic pressure and volume relationship (Klotz curve). For all patients, the LV end-diastolic pressure was unavailable and was estimated by the pulmonary capillary wedge pressure (PCWP) computed using Nagueh's formula in Eqn. (6) [38]:

$$\text{PCWP} = 1.24 \times (E/e') + 1.9, \tag{6}$$

where E is the mitral inflow velocity and e' is the average of the septal and lateral annular velocities. The LV PCWP for each patient is provided in Table 1.

The sequential least-squares algorithm was used to minimise the error between the LV end-diastolic pressure predicted with the FE model and estimated from the patient's Klotz curve:

$$min\ \Phi_1(A,B) = \sum_{i}^{N} (P_i - \bar{P}_i)^2 + (\text{EDV} - \overline{\text{EDV}})^2, \tag{7}$$

where N is the total number of points on the pressure-volume curve, P_i and EDV are FE predictions, and $\bar{P}_i$ and $\overline{\text{EDV}}$ are from the patient's clinical records. A scalar (A) and an exponential multiplier (B) were used to uniformly scale the linear (a_i) and exponential (b_i) terms, respectively, in Eqn. (1). All initial parameters were the same for all PPCM models before optimisation. Initial passive material parameters were those of a healthy myocardium calibrated by Sack [32] using experimental tri-shear data from Sommer [39]. The initial parameters were a = 1.05 kPa, b = 7.542, a_f = 3.465 kPa, b_f = 14.472, a_s = 0.481 kPa, b_s = 12.548, a_{fs} = 0.283 kPa, and b_{fs} = 3.088. After optimisation, the mean square error of the Klotz and *in silico* pressure values was computed.

2.5.2. Active mechanical properties

The contractility scaling factor T_{max} was optimised so that the models produced clinically recorded stroke volumes. The initial T_{max} was 100 kPa for all models. The LV long-axis shortening (LVLS) was included in the objective function, Eqn. (8), to ensure physiological deformation during contraction as observed in the cMRI data for each patient. The sequential least-squares optimisation algorithm in Python was used with Abaqus as a forward solver:

$$min\ \Phi_1(A,B) = (SV - \overline{SV})^2 + (LVLS - \overline{LVLS})^2\ , \tag{8}$$

where SV and LVLS are FE predicted stroke volume and LV long-axis shortening, and $\overline{\text{SV}}$ and $\overline{\text{LVLS}}$ are the corresponding clinical *in vivo* values. $\overline{\text{LVLS}}$ was calculated with [40]:

$$\overline{LVLS} = \frac{(L_4 + L_2)}{2}, \tag{9}$$

with

$$L_4 = 100\left(1 - \frac{L_{4\mathrm{ES}}}{L_{4\mathrm{ED}}}\right), \tag{10}$$

$$L_2 = 100\left(1 - \frac{L_{2\mathrm{ES}}}{L_{2\mathrm{ED}}}\right), \tag{11}$$

where L_4 and L_2 are the long-axis shortening in the 4-chamber and 2-chamber view, respectively. L_{4ED} and L_{2ED} are the lengths at end-diastole while L_{4ES} and L_{2ES} were the lengths at end-systole. The values were manually extracted from cine cMRI sequences from the respective chamber views.

2.6. Circulatory system and simulation of cardiac cycles

2.6.1. Models without LVAD

A circulatory system comprising pulmonary and systemic circuits was coupled to the biventricular models as described by Sack [32]. The coupling of the lumped circulatory system and the mechanical function was carried out in Abaqus. Compliance and resistance parameters represented fluid flow between pulmonary circuit (C_{PA} and C_{PV}), heart, and systemic circuit (C_{SA} and C_{SV}) (Figure 1 c).

A brief description of the volume, pressure, compliance, resistance and fluid exchange relationship within the circulatory system is provided. Additional information can be found in the Abaqus Theory Guide [41]. Equation (12) describes the relationship between the volume V_i, pressure P_i and compliance k_i in the fluid cavity chamber i.

$$V_i(t) = V_i(0) + k_i P_i(t), \tag{12}$$

Unidirectional flow between compliance vessels was governed by pressure gradients in Eqn. (13):

$$Q(t) = \frac{dV}{dt} = \frac{1}{R}\frac{dP}{dt}, \tag{13}$$

where Q is the flow, V is the volume, P is the pressure and R is the resistance. During contraction, pressure increases in the ventricles and flow was permitted when it exceeds the pressure in the connected outflow chamber. Volume in the circulatory system was assumed to be constant.

Each compliance vessel was loaded with fluid until the LV reached end-diastolic pressure and volumetric conditions before the first cardiac cycle was initiated. The cardiac cycle comprised active contraction (480 ms) and passive filling (300 ms), corresponding to a heart rate of 77 beats per minute. Six cardiac cycles were simulated to facilitate convergence of the pressure-volume curve.

2.6.2. Implementation of LVAD support

To simulate LVAD support, a secondary connection from the LV to the systematic circuit was added in the circulatory model (Figure 1 c). The flow in the secondary connection, i.e., the LVAD, was continuous and unidirectional, and introduced fluid exchange between LV cavity and arterial system.

Only the effects of the LVAD were simulated, and fluid flow from the LV and the LVAD contributed to the arterial system.

The output from the LVAD to the arterial system was varied to simulate operational speeds of the LVAD of 8,000, 9,000, 10,000, 11,000 and 12,000 revolutions per minute (rpm). For each speed, the flow rate profile was coupled to the pressure difference between inflow and outflow cavities to which the pump connected. The profiles were based on experimental flow rates of the Heartmate II™ LVAD for pressure differences varying between 0 and 200 mmHg described by Sack [22]. Apart from the LVAD, all other fluid exchanges between cavities in the computational models were driven by pressure differences. For models with LVAD support, ten cardiac cycles were simulated to reach convergence of the pressure-volume curve.

2.7. Data and statistical analysis

Results from end-diastole and end-systole of the 6th and 10th cardiac cycle were analysed for models without and with LVAD support, respectively. In addition to the active contraction, fluid exchanges in the circulatory system are driven by pressure differences between cavities. Introduction of the LVAD support changes conditions in the system and as a result, more cardiac cycles are needed to achieve convergence compared to the non-LVAD models. Pressure and volume values of the converged solutions and the preceding cycle (last two cycles) were compared. End-diastole and end-systole were determined from the pressure-volumes curves as time points before isovolumetric contraction and isovolumetric relaxation, respectively.

The terms ‘average’ and ‘group average’ interchangeably refer to the arithmetic mean computed using values of more than one model, e.g., several patients of a group. In contrast, the terms ‘mean’ or ‘patient mean’ interchangeably refer to the arithmetic mean computed from elements values of the same model, i.e., patient.

Results from models without (untreated) and with LVAD (treated) were compared and statistical analyses performed for all patients. Due to the small sample size in the groups with recovered and non-recovered patients, no statistical comparisons involving these groups were performed.

Myofibre strains and stresses were normalised by element volume to eliminate potential effects from different element sizes. The volumetric averaged value σ_{iv} for element i was calculated using Eqn. (14),

$$\sigma_{iv} = \frac{v_i}{V_\mu}\sigma_i \tag{14}$$

where v_i is the volume of element i, V_μ is the mean volume for all elements, and σ_i is the stress or strain value of element i in the model.

Considering all patients, average myofibre stress and strains statistical comparisons were performed between models without the LVAD support and models with the LVAD support at a particular speed of 8,000, 10,000 and 12,000 rpm.

Results were reported as mean ± standard deviation (SD) or as median (interquartile range). Statistical tests used include the Shapiro–Wilk and Kolmogorov Smirnov test for normality. Parametric tests used included the Student t-test and Welch test and non-parametric tests included the Kruskal Wallis test and Wilcoxon signed-rank test. All statistical tests were two tailed and the Bonferroni correction was applied in all pairwise comparisons. Significance was considered at $p < 0.05$.

3. Results

3.1. Optimisation of material parameters

The optimisation algorithm for the passive material parameters produced *in silico* end-diastolic volumes that closely matched the target in vivo values (Table 3). However, the Klotz method LV underestimated the unloaded volume (V_{0K}) compared to the unloaded volume of the LV geometry (V_0)Table 3. This discrepancy increased with increase in V_0.

The optimisation yielded substantially higher scalars $A > 9$ and lower exponential multipliers $B < 0.4$ than for models R45A and N39A which resulted in linear end-diastolic pressure-volume *in silico* curves for patients R20A, N18A, N12A and N06D. However, Klotz [37] clearly stated that end-diastolic pressure-volume relationships are known to have in common a non-linear convex shape irrespective of the species or heart condition. To improve models R20A, N18A, N12A and N06D, the optimisation algorithm for these four models was revised by (i) assigning $B = 1.6822$ as the average value from models R45A and N39A and (ii) changing the error function to the squared difference between the predicted and the patient-specific end-diastolic volume. This produced lower values for A for all four models (Table 3) and more non-linear end-diastolic pressure-volume curves, particularly for R20A and N18A.

Table 3: LV unloaded volumes, optimised material parameters, and the relative error in the end-diastolic volume and the mean squared error (MSE) of the LV end-diastolic pressure values obtained from comparisons between the *in silico* model and the target patient's Klotz curve. V_{0K}: Unloaded left ventricular volume determined with Klotz method, V_0: unloaded left ventricular volume based on ventricular geometry, A: scalar multiplier, B: exponential multiplier from initial optimisation algorithm A_{mod}: scalar multiplier and B_{mod}: exponential multiplier from modified optimisation algorithm and MSE: Mean squared error for LV pressure (Klotz curve versus *in silico* curve).

Patient	V_0 **(ml)**	V_{0K} **(ml)**	A	B	A_{mod}	B_{mod}	**EDV Error (%)**	**MSE (mmHg)**	T_{max} **(kPa)**
R45A	60	59	0.1000	1.8485	-	-	1.7857	1.0019	154
N39A	82	62	1.2270	1.5159	-	-	0.7407	0.3392	135
R20A	134	87	9.7529	0.3109	6.2000	1.6822	0	3.5994	200
N18A	152	87	28.8488	0.1000	14.2239	1.6822	0	6.5459	233
N12A	203	116	28.8500	0.1000	21.015	1.6822	0	15.1984	187
N06D	174	85	133.1495	0.1000	59.5059	1.6822	0	69.6533	110

The final LV end-diastolic pressure-volume curves for each model after optimisation are displayed in Figure 1 b). The volume was normalised to the unloaded state to compare the relative increase during the filling phase. Qualitatively, the slope and linearity of the curves increased with a decrease in the volume entering the LV during passive filling (i.e., EDV-ESV). Models R45A and N39A exhibited more compliant LVs than R20A, N18A, N12A and N06D, which had the stiffest LV, i.e. LV compliance increased with an increase in ejection fraction.

The active material optimisation yielded an average T_{max} of 170 ± 45 kPa, ranging from 110 kPa for N06D to 233 kPa for N39A (Table 3).

Convergence of the optimised models was reached at the 6th and 10th cardiac cycle for models without and with LVAD support, respectively, Figure 2.

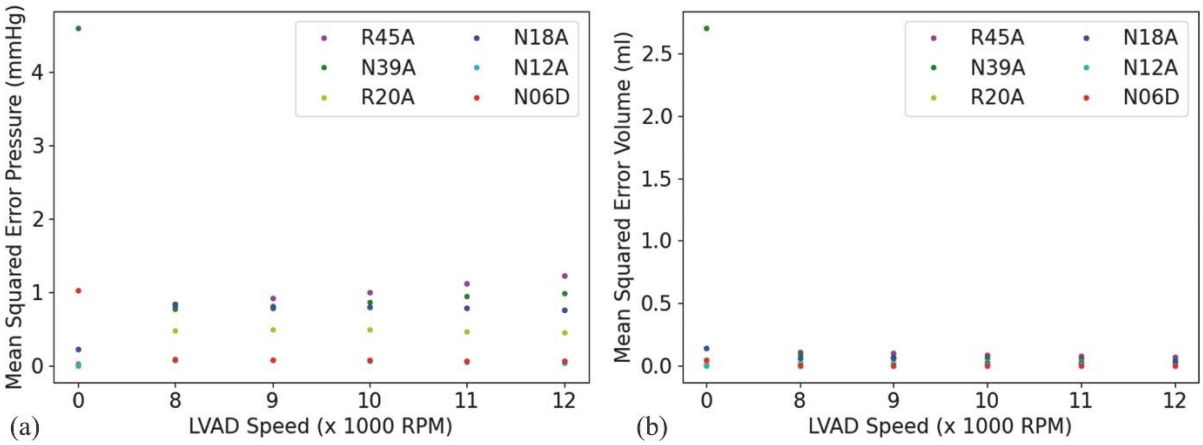

Figure 2: Mean square error of LV pressure (a) and LV volume (b) for the last two cardiac cycles for each PPCM patient. Zero revolution per minute represents models without LVAD.

3.2. Cardiac function

3.2.1. Ventricular volumes and pressures

Models without LVAD accurately matched the *in vivo* LVEF and volume (from the patient's clinical records) (Table 4 and Figure 3 a). For each patient, the target end-systolic *in vivo* volume was the V_0 after segmentation (Table 4), and the end-diastolic volume was derived using clinical EF and V_0. However, the predicted LV end-diastolic pressure deviated from the *in vivo* value by 21.2% ± 5.4%, -10.1% ± 2.1%, and 2.0% ± 15.6% for patients with an LVEF > 20%, LVEF < 20%, and all patients, respectively (Figure 3 b).

Table 4: Functional and dimensional parameters of LV and RV. Unloaded ventricular volume V_0 of reconstructed cardiac geometries, end-diastolic volume (EDV) calculated using clinically recorded ejection fraction (*in vivo* EF) and V_0, and ejection fraction predicted with finite element models (*in silico* EF).

Patient	LV V_0 (ml)	LV EDV (ml)	LVEF *in vivo* (%)	LVEF *in silico* (%)	RV V_0 (ml)	RV EDV (ml)	RVEF *in vivo* (%)	RVEF *in silico* (%)
R45A	60	110	45	45.0	64	123	48	27
N39A	82	135	39	39.0	42	102	59	48
R20A	134	168	20	20.0	88	111	21	26
N18A	152	185	18	17.0	79	99	20	27
N12A	203	231	12	12.0	150	-	-	15
N06D	174	110	6	6.0	104	113	8	8

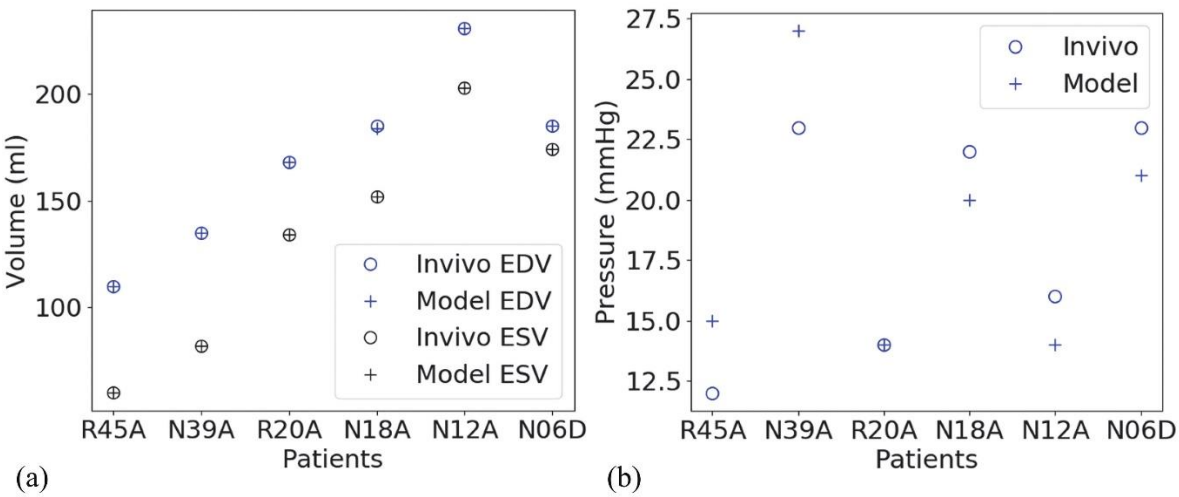

Figure 3: Comparison of *in vivo* and predicted LV volume and pressure. The models accurately replicated *in vivo* end-diastolic and end-systolic volumes (a) but overestimated and underestimated the end-diastolic pressure (b) for patients with EF > 20% and < 20%, respectively.

In models with LVAD support, the LV end-diastolic volume was lower than that without LVAD support (Student's paired t-test, $p \geq 0.124$). The 8,000 rpm LVAD yielded the lowest reduction in average LV end-diastolic volume of -9.0 ± 6.9 ml (n = 6, $p = 0.141$) whereas the 12,000 rpm LVAD yielded the highest reduction of -15.8 ± 13.8 ml for all models ($p = 0.190$).

The average RV end-diastolic volume of models with LVAD support increased marginally compared to those without LVAD support ($p \geq 0.0758$, n = 6, Student's paired t-test) except patient R45A who had slight increases of -0.8% at higher speeds of 11,000 and 12,000 rpm.

Compared to models without LVAD support for all patients, an increasing reduction in the average LV end-diastolic pressure was observed for increasing LVAD speeds, namely from -5.5 ± 3.4 mmHg ($p = 0.0531$) at 8,000 rpm to -8.7 ± 3.4 mmHg ($p = 0.00819$) at 12,000 rpm (n = 6, Student's paired t-test).

The average RV end-diastolic pressure for all models increased slightly with the 8,000 rpm LVAD support (2.0 ± 0.5166 mmHg, $p = 0.300$) compared to no LVAD support. There was no change for the 10,000 rpm but there was a slight decrease for models with LVAD speeds of 9,000, 11,000 and 12,000 rpm (-0.7 ± 0.5164 mmHg, $p < 4.165$).

3.2.2. Pressure-volume loops

The LV pressure-volume loops became triangular with LVAD compared to no LVAD, i.e. do not feature isovolumetric phases, and triangularity increases with increasing LVAD speed (Figure 4 a). The LV pressure-volume loops of models with low ejection fraction (N18A, N12A and N06A) shifted more downwards and to the left than of models with higher ejection fraction (R45A and N39A). There was a noticeable rightward shift of the RV end-diastolic volume for the non-recovered patients (N39A, N18A, N12A and N06D), whereas marginal changes were observed for the recovered patients (R45A and

R20A). Of note are the RV pressure-volume loops for model R45A, which were further to the right with higher end-diastolic volumes than the LV curves of 125 (IQR 0.75) ml versus 110 (IQR 0.75) ml, respectively, (p = 0.031, n = 6, Wilcoxon sign rank test).

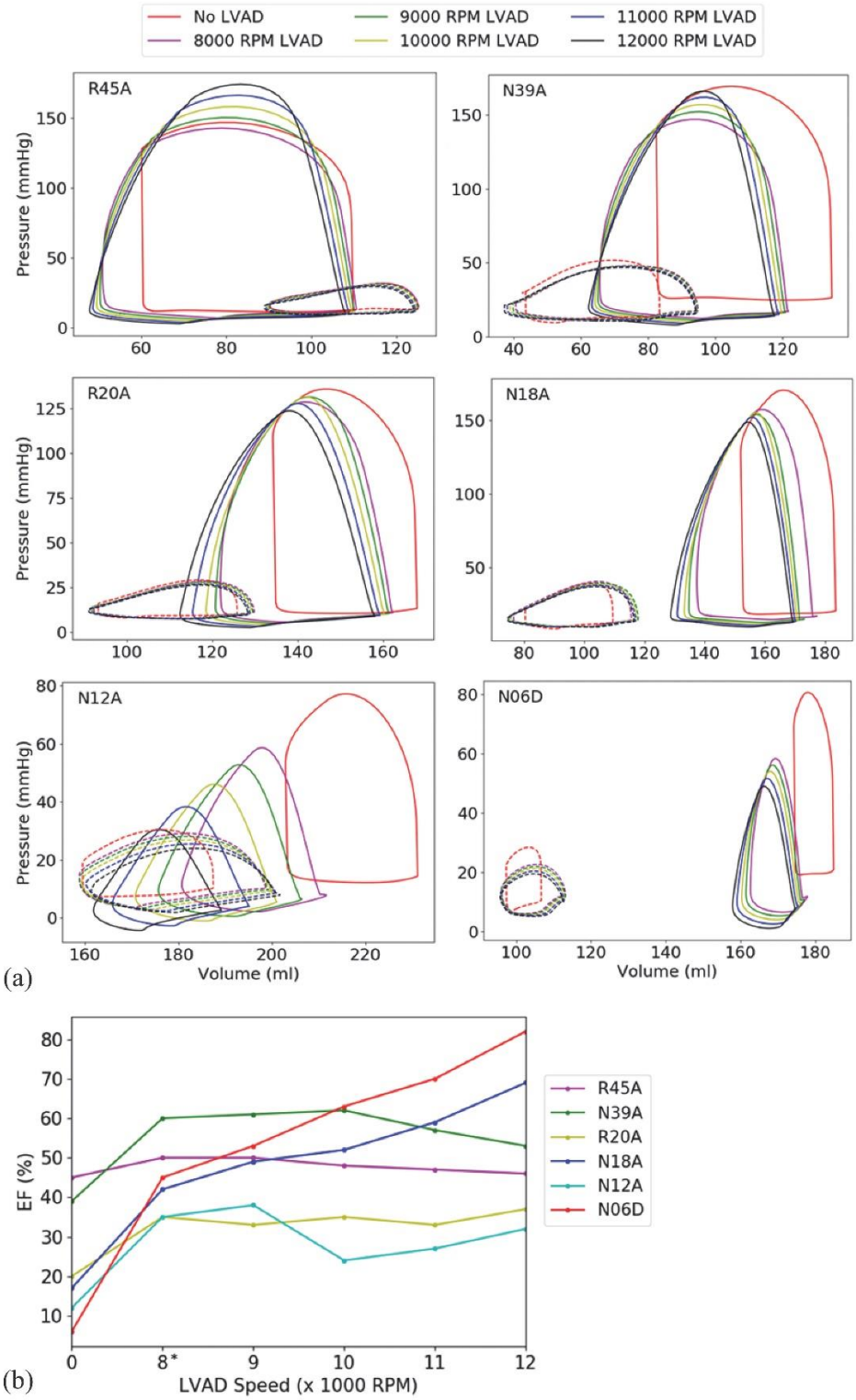

Figure 4: a) Pressure-volume loops for the LV (solid lines) and RV (dashed lines) versus LVAD speed for all patients. Apart from R45A, the LV pressure-volume curve shifted to the left and downwards, whereas the RV pressure-volume curve shifted to the right after implementing the LVAD support. b)

Changes in the LV ejection fraction (EF) with an increase in LVAD speeds. The zero revolutions per minute (RPM) on the horizontal axis represents models without the LVAD. Increasing the LVAD speeds led to a steady increase in EF in some models, while there was a decrease or marginal change in EF in others. * Indicates significant differences between the average ejection fraction for models without and with LVAD at each speed ($p < 0.05$).

3.2.3. Ejection fraction

Implementing the LVAD in the models resulted in the LVEF (i) steadily increasing (N18A and N06D), (ii) fluctuating (R20A and N12A), (iii) reaching a maximum at an intermittent LVAD speed (N39A), and (iv) steadily decreasing (R45A) with LVAD speeds increasing from 8,000 to 12,000 rpm, see Figure 4 b. For the LVAD with 8,000 rpm compared to no LVAD support, the average LVEF improved by 21.3 ± 11.3 per cent points for all models ($p = 0.0283$, n = 6, Student's paired t-test), see Table 4. For LVAD speeds above 8,000 rpm, there were slight increases in the average LVEF ($p \geq 0.0505$) for all patients.

Noteworthy, PPCM patients had a lower average EF in the LV than the RV without LVAD, whereas the average EF was higher in the LV than the RV with LVAD support, irrespective of the LVAD speed.

The average LV cardiac output improved with LVAD compared to no LVAD for all patients (2.7 ± 1.2 L/min) and ranged from 5.3 ± 0.9 L/min to 6.3 ± 3.0 L/min for 8,000 to 12,000 rpm LVAD speed, ($p > 0.0156$, n = 6, Student's paired t-test).

Table 5: Average LV and RV ejection fraction (EF) without LVAD and with LVAD at different speeds for all patients (n = 6). * Represents statistical significance with $p < 0.05$ for pairwise comparisons with models without LVAD at each LVAD speed including Bonferroni correction.

LVAD Speed (x1000 rpm)	**LV EF (%)**	**RV EF (%)**
None	23.2 ± 15.5	25.2 ± 13.6
8	44.5 ± 9.57*	29.3 ± 14.7
9	47.3 ± 10.2	30.0 ± 15.0
10	47.3 ± 15.4	31.3 ± 15.3
11	48.8 ± 16.4	31.2 ± 15.9
12	53.2 ± 19.2	31.2 ± 16.4

3.2.4. LVAD contribution to stroke volume

The average LV stroke volume increased with LVAD compared to no LVAD (Figure 5, $p > 0.0819$, n = 6, Student's paired t-test). For the 8,000 rpm LVAD compared to no LVAD, the increase in LV stroke

volume increased with decreasing EF of the patients. The lowest and highest increase was observed for patients R45A (10%) and N06D (655%).

The LV and the LVAD jointly contributed to the stroke volume in models with higher EF (R45A, N39A, R20A and N18A), whereas the LVAD was the only contributor in the models with the two lowest EF (N12A and N06D). For joint contribution to stroke volume, the LV contribution decreased with a decrease in EF amongst models and with an increase in LVAD speed for each model.

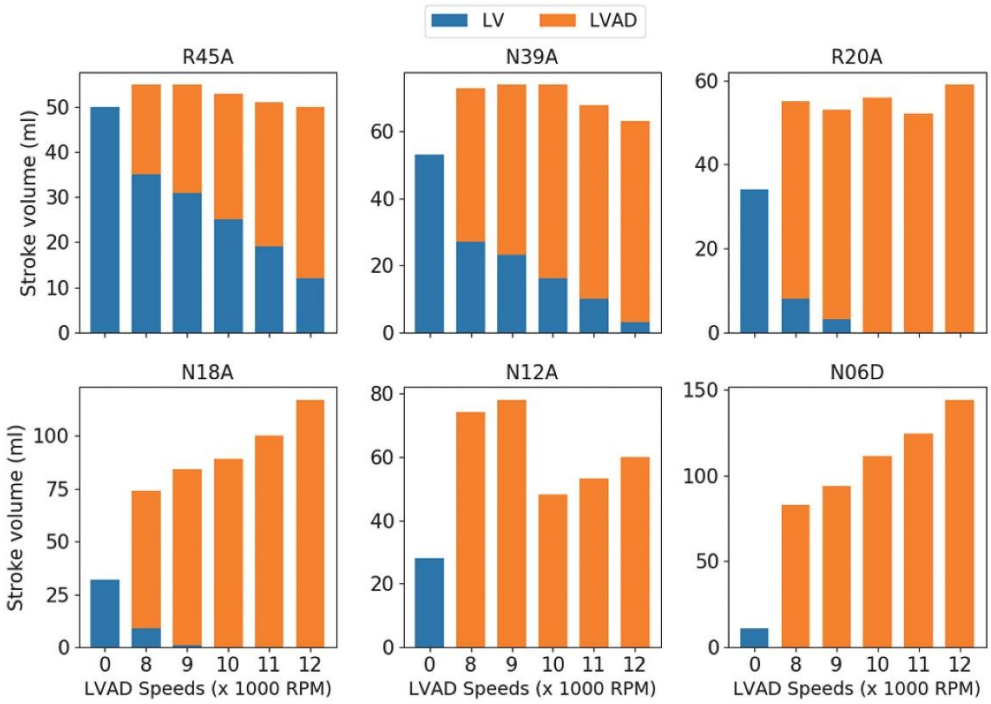

Figure 5: Variation of LV stroke volume contributions with LVAD speed for each PPCM model and zero revolutions per minute (RPM) represents PPCM models without the LVAD. The LV and the LVAD jointly contributed to stroke volume in the four models with EF = 18% and higher, while the LVAD was the only contributor in the two models with the lowest EF of 12% and 6%.

3.3. Myofibre stress

3.3.1. Individual patients

The LV myofibre stress distribution (i.e. probability density curve) for models without LVAD support was different compared to models with LVAD support but did not change with LVAD speed for each patient except R45A (Figure 6). For the latter, the stress distribution with and without LVAD were similar at end-diastole. For each patient, the peak probability density was higher with LVAD support than without and increased with increasing LVAD speed.

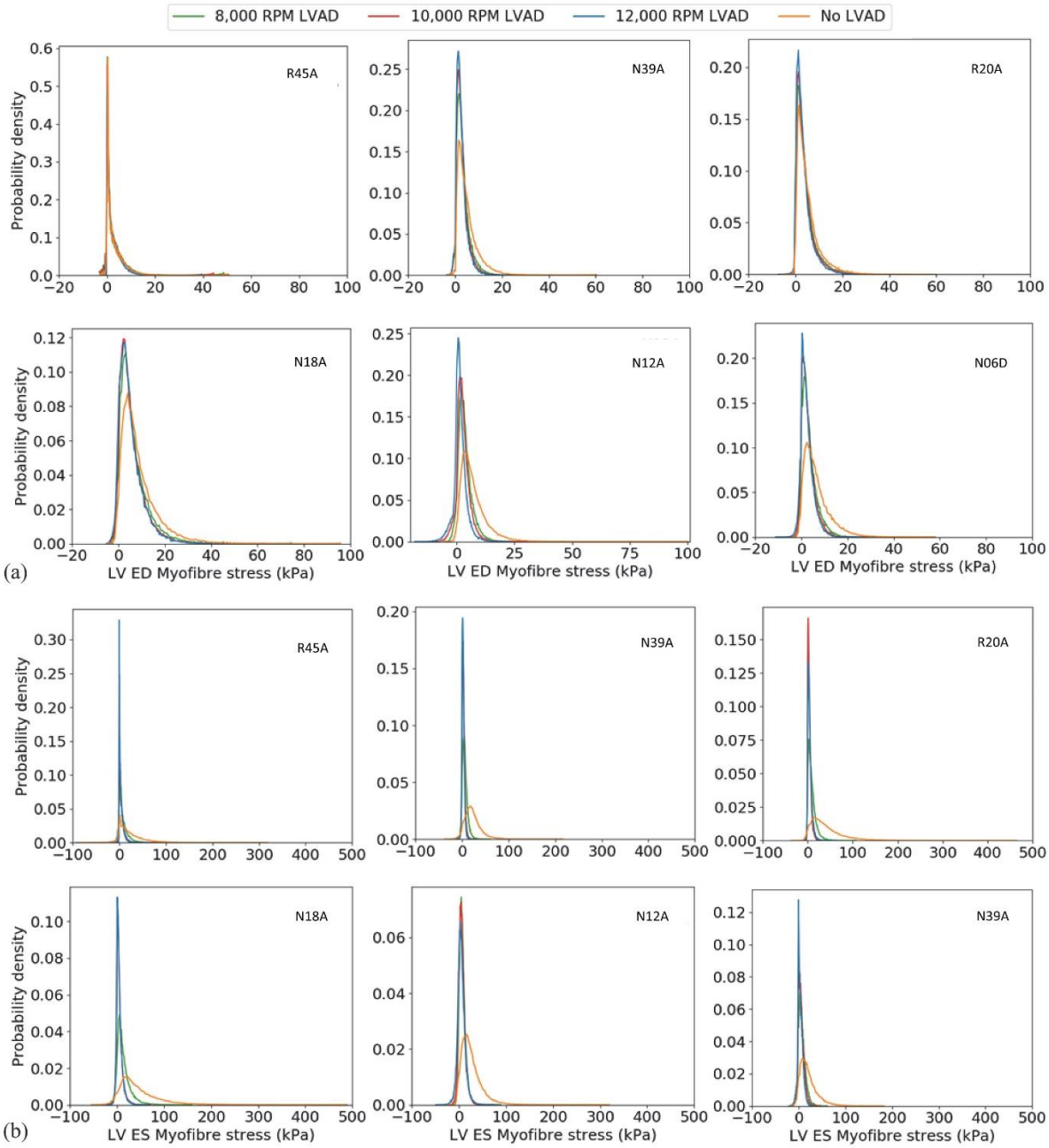

Figure 6: Probability density curves showing the LV myofibre stress distribution for each patient at (a) end-diastole (ED) and (b) end-systole (ES). LV myofibre stress distribution was different for models without LVAD support but similar for different LVAD speeds for each patient except R45A. For that patient, similar stress distributions were predicted with and without LVAD at end-diastole. The peak probability density was higher with than without LVAD support and increased with increasing LVAD speed.

The two main observations for myofibre stress contour plots were (see representative plots for R45A and N06D in Figure 7):

- The end-diastolic myofibre stress decreased from no LVAD to LVAD support at 8,000 rpm and decreased from 8,000 to 12,000 rpm LVAD speed, whereas the end-systolic myofibre stress

decreased from no LVAD to LVAD at 8,000 rpm but increased from 8,000 rpm to 12,000 rpm LVAD speed. This was observed for models R45A and N39A.

- For models R20A, N18A, N12A and N06D, the end-diastolic and end-systolic myofibre stress decreased from no LVAD to LVAD at 8,000 rpm and further decreased from 8,000 rpm to 12,000 rpm. This decrease in myofibre stress with increasing LVAD speed was smaller for R20A and N18A than for N12A and N06D.

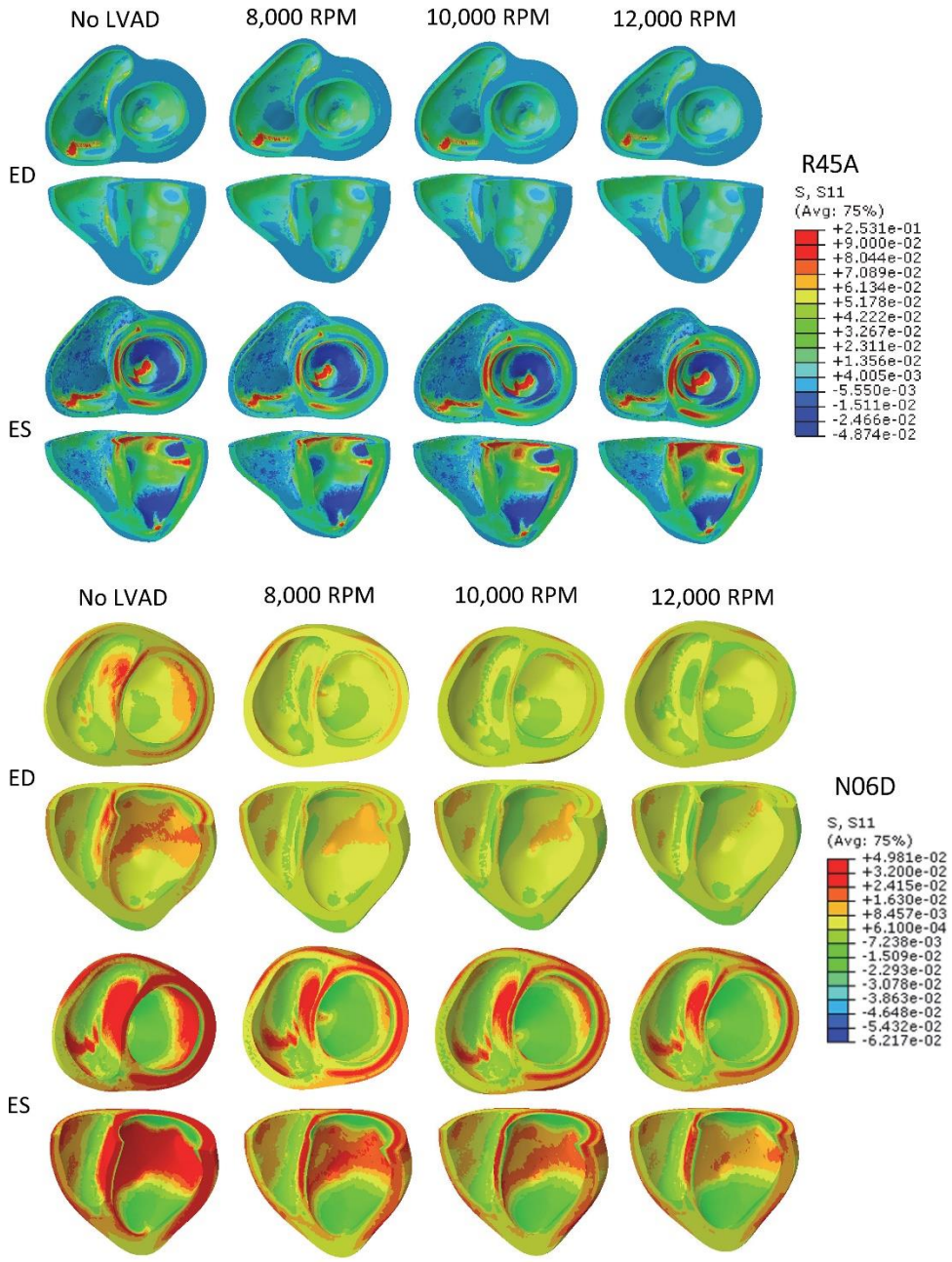

Figure 7: Representative contour plots displaying the two main trends of the biventricular myofibre stress in PPCM with increasing LVAD speed at end-diastole (ED) and end-systole (ES). Model R45A illustrates the first trend with a decrease in myofibre stress with an increase in LVAD speed at end-diastole but an increase in myofibre stress from 8,000 to 12,000 rpm at end-systole. This was observed for models R45A and N39A. Model N06D illustrates the second trend with a decrease in myofibre

stress with increasing LVAD speed both at end-diastole and end-systole, observed for models R20A, N18A, N12A and N06D.

3.3.2. All patients

The patient mean myofibre stress in LV and RV decreased with LVAD compared to without LVAD for each patient, except for the RV end-diastolic myofibre stress that exhibited only marginal changes (Figure 8).

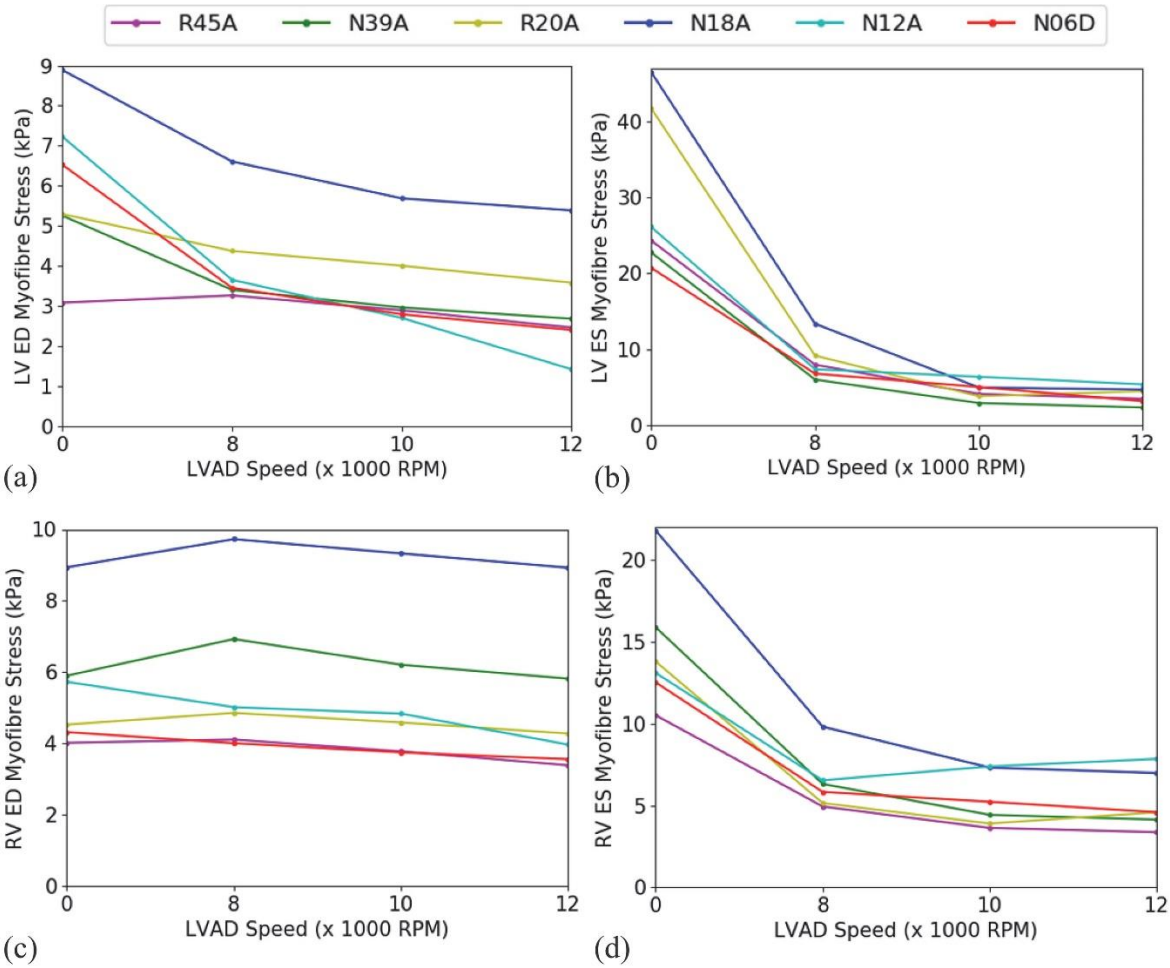

Figure 8: Patient mean myofibre stresses versus LVAD speed in LV and RV at end-diastole (ED) and end-systole (ES). The LVAD support led to a decrease in myofibre stress in the LV at end-diastole (a) and end-systole (b) but in the RV only at end-systole (d) and not at end-diastole (c). Zero revolution per minute (RPM) represents models without the LVAD.

In the LV at end-systole, the average myofibre stress was significantly lower with LVAD than without LVAD (between 3.6-fold decrease at 8,000 rpm and 7.7-fold decrease at 12,000 rpm, $p < 0.00661$, n = 6, Student's paired t-test), whereas the decrease was smaller at end-diastole (between 1.4-fold at 8,000 rpm and 2-fold at 12,000 rpm, $p > 0.938$, n = 6, Wilcoxon signed-rank test), Table 6.

Similar to the observation for the LV, RV average myofibre stress was predicted to be significantly lower for models with LVAD than without LVAD at end-systole (between 2.3-fold decrease at 8,000 rpm and 2.8-fold decrease at 12,000 rpm, $p \leq 0.00348$, n = 6, Student's paired t-test). At end-diastole,

the RV average myofibre stress was not significantly different with and without LVAD support (no change at 8,000 rpm and a 1.1-fold decrease at 12,000 rpm, $p \geq 1.31$, n = 6, Student's paired t-test).

Table 6: Average LV and RV myofibre stress for all patients at end-diastole and end-systole at different LVAD speeds. *Statistical significance for comparison with models without LVAD ($p \leq 0.01$).

LVAD Speed	End-diastole		End-systole	
(x1000 rpm)	LV (kPa)	RV (kPa)	LV (kPa)	RV (kPa)
0	6.05 ± 1.98	5.57 ± 1.82	30.35 ± 10.90	14.62 ± 3.94
8	4.13 ± 1.28	5.78 ± 2.20	8.47 ± 2.63*	6.43 ± 1.77*
10	3.51 ± 1.17	5.42 ± 2.12	4.57 ± 1.20*	5.32 ± 1.67*
12	3.00 ± 1.36	4.99 ± 2.12	3.95 ± 1.12*	5.26 ± 1.76*

3.4. Myofibre strain

3.4.1. Individual patients

As observed for myofibre stress, the LV myofibre strain probability density was different without and with LVAD but similar for different LVAD speeds at end-diastole and end-systole; except for patient R45A at end-diastole with similar strain probability curves with and without LVAD.

Two trends were observed from contour plots of biventricular myofibre strain (Figure 9):

- The end-diastolic myofibre strain decreased from no LVAD to LVAD support at 8,000 rpm and decreased from 8,000 to 12,000 rpm LVAD speed, whereas the end-systolic myofibre strain decreased from no LVAD to LVAD support at 8,000 rpm but increased marginally with increasing LVAD speed from 8,000 to 12,000 rpm. This was observed for patient R45A.
- For the other five patients, the end-diastolic and end-systolic myofibre strain decreased from no LVAD to the LVAD at 8,000 rpm and decreased from 8,000 to 12,000 rpm LVAD speed.

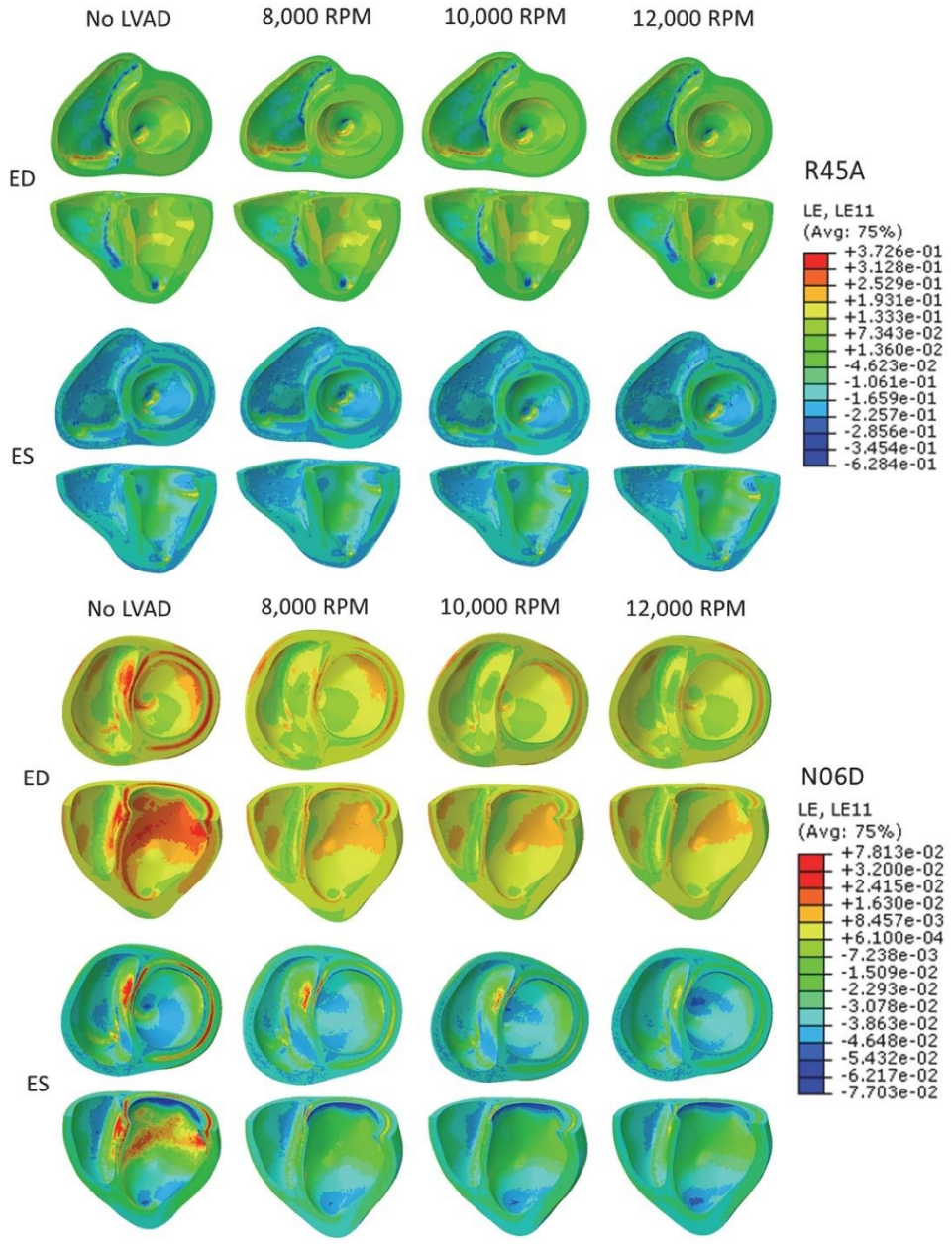

Figure 9: Representative contour plots displaying the two main trends of the biventricular myofibre strain distribution for the PPCM patients with and without the LVAD support at end-diastole (ED) and end-systole (ES). For patient R45A, end-diastolic myofibre strains decreased from no LVAD to the LVAD at 8,000 rpm and decreased further from 8,000 to 12,000 rpm LVAD speed. At end-stole, the myofibre strains decreased from no LVAD to the LVAD at 8,000 rpm but increased marginally with increasing LVAD speed from 8,000 to 12,000 rpm. For the other patients, represented by patient N06D, end-diastolic and end-systolic myofibre strain decreased from no LVAD to the LVAD at 8,000 rpm and decreased further from 8,000 to 12,000 rpm LVAD speed.

3.4.2. All patients

Marginal changes in the patient mean myofibre strain in LV and RV were observed with LVAD support compared to no LVAD. In the LV, the average myofibre strain was slightly lower with LVAD support than without the LVAD support at end-diastole and end-systole for the 8,000 rpm and 10,000 rpm

LVAD ($p \geq 0.0764$Table 7), whereas for the 12,000 rpm, there was a significant decrease at end-diastole ($p = 0.0385$) and a slight increase at end-systole ($p = 2.543$), Table 7.

In the RV, the average myofibre strain marginally decreased with LVAD compared to no LVAD at end-diastole and end-systole for the 10,000 rpm and 12,000 rpm LVAD ($p \geq 0.0647$), whereas for the 8,000 rpm, there was a slight increase at end-diastole ($p = 2.5314$) and a slight decrease at end-systole ($p = 0.0293$).

Table 7: Average LV and RV myofibre strain for all patients at end-diastole and end-systole for models without LVAD and with LVAD at different speeds. *Statistical significance for comparison with the model without LVAD ($p < 0.05$, n = 6, Student's paired t-test).

LVAD Speed	**End-diastole**		**End-systole**	
(x1000 rpm)	**LV (%)**	**RV (%)**	**LV (%)**	**RV (%)**
None	4.38 ± 3.31	2.37 ± 2.19	-6.68 ± 3.51	-8.94 ± 4.30
8	3.86 ± 3.49	2.41 ± 2.23	-6.52 ± 3.44	-7.19 ± 3.85*
10	3.64 ± 3.47	2.33 ± 2.17	-6.30 ± 3.04	-6.60 ± 3.38
12	3.41 ± 3.43*	2.26 ± 2.13	-6.76 ± 3.00	-6.98 ± 3.34

4. Discussion

This study investigated how disease severity affected the efficacy of partial LVAD support in South African PPCM patients using patient-specific finite element modelling to provide insights into therapeutic mechanisms for personalised LVAD treatment in PPCM.

4.1. Optimisation of material parameters

The mean passive material parameters for all PPCM patients, i.e. A = 17.05 ± 22.28 kPa and B = 1.68 ± 0.11, were substantially higher than those reported for the healthy model (A = 0.65 kPa and B = 1.00) [42] and heart failure model (A = 8.00 kPa and B = 4.00) [22]. This could imply that the LV myocardium is stiffer in PPCM than in the healthy case and in heart failure. The mean active tension parameter of the PPCM models (T_{max} = 170 ± 45 kPa) was higher than that for a healthy human heart (T_{max} = 143 ± 11.1 kPa) [43] but same as the T_{max} = 170 kPa reported for heart failure in humans [22].

The method by Klotz [37] has been used to estimate a patient's LV end-diastolic pressure-volume relationships but it underestimated the initial volumes (V_0) for PPCM patients (Table 3). These discrepancies were observed in previous studies for example, 2.92% [44], 38% [32] and 32% [22]. In another study by Dabiri [42], the initial volume was constrained to the V_{0K} determined the Klotz method. Patient N06D with the highest V_0 versus V_{0K} discrepancy yielded the highest optimisation mean squared error (Table 3). Therefore, there is need to improve the calibration of patient-specific passive material parameters for patients with similar characteristics.

Despite the limitations in the optimisation of material parameters, simulation results from the converged solutions of the optimised patient-specific models representing PPCM patients produced cardiac function metrics similar to the target in vivo metrics, see Table 4 and Figure 3.

4.2. Cardiac function

LVAD support decreased end-diastolic volumes and pressures in the LV for all models but increased either the volume or pressure in the RV for some models except R45A. These changes were amplified with increasing LVAD speed, indicated by the left and downward shift of the LV and the rightward shift of the RV pressure-volume loops, particularly for models with lower LVEF (N18A, N12A and N06A, Figure 4 a). The LV pressure-volume loops becoming more triangular in shape is a sign of continuous unloading of the LV by the LVAD during the isovolumetric phases of the cardiac cycle (Figure 4 a), consistent with findings by Sack [22].

While LVAD provides haemodynamic unloading of the LV, the resultant increase in systemic blood flow increases RV workload, left septal shift and RVEDV, altering RV geometry and function [22, 45]. For this reason, RV failure is often a contraindication to eligibility for LVAD in patients.

In the current study, there was an increase in RV end-diastolic volume due to LVAD support which resulted in an increase in RV ejection fraction except for patient R45A. Interestingly, patient R45A experienced decreases in RV end-diastolic volumes (-0.8%) and pressures (-13%) at high LVAD speeds (11,000 - 12,000 rpm) compared to models without LVAD. This may indicate better RV compliance and capacity to adapt at higher LVAD speeds for models with higher ventricular ejection fraction at baseline (LVEF: 45% and RVEF: 48%, Table 4). Modelling could, therefore, potentially determine the likelihood of myocardial recovery with LVAD or drug therapy, in addition to determining patient-specific LVAD speeds that would be less likely to incur worsening RV failure.

The improvements in the LVEF due to LVAD treatment predicted for PPCM (between 21 ± 11.3 per cent points at 8,000 rpm and 30 ± 28.2 per cent points at 12,000 rpm) were greater than those reported for chronic heart failure (between 0.9 per cent points at 8,000 rpm and 6.5 per cent points at 12,000 rpm) [22]. For some patients, the improvement in LVEF reached a maximum at an intermediate LVAD speed and declined or fluctuated for further increasing speed (Figure 4 b). These findings suggest the existence of patient-specific and/or disease-specific optimal LVAD speeds and emphasises the importance of computational modelling to advance personalised LVAD treatment in patients with heart failure.

PPCM patients benefited functionally from LVAD treatment, with a larger EF predicted for the LV than the RV with the LVAD support similar to the healthy case [30] compared to the lower EF in the LV than the RV in models without LVAD support (Table 5). This further illustrates the ability of the LVAD to provide more benefits for patients with lower LVEF than those with higher LVEF.

The lowest LVAD speed of 8,000 rpm was sufficient for all PPCM patients to achieve an LV cardiac output within the reference range of 3.3 - 7.3 L/min for healthy women [46], namely between 4.24 L/min for R45A (with the highest EF) and 6.40 L/min for N06D (with the lowest EF). However, only the highest LVAD speed of 12,000 rpm increased the average LVEF (53.2% ± 19.2%) close to the reference value of LVEF ≥ 54% for healthy women [30, 47].

The LV and LVAD co-contributed to the stroke volume for four patients with LVEF ≥ 18%. For these patients, the proportion of the LV contribution decreased with increasing LVAD speed and the LVAD was the sole contributor to LV output at higher speeds from 10,000 rpm for patient N18A and 11,000 rpm for patient R20A with LVEF = 18% and 20%, respectively (Figure 5). For patients with the lowest LVEF of 6% and 12%, the LVAD solely provided the ventricular output at all speeds. These findings concur with a previous study that suggested that mechanical support from the LVAD at high speeds (12,000 rpm) excessively reduces LV volume and results in reduced cardiac output compared to lower LVAD speeds [22]. The relationship between LVAD speed and the work required by the patient's ventricle may affect the functional recovery of the LV. Therefore, patient-specific selection of the LVAD speed and adjustment during the recovery process to allow for increasing ventricular function may offer the potential to achieve optimal support in PPCM.

4.3. Myocardial stress

LVAD support resulted in a substantial reduction in end-systolic LV myofibre stress from 30.4 ± 10.90 kPa to between 8.5 ± 2.6 kPa and 3.95 ± 1.1 kPa (for 8,000 and 12,000 rpm, respectively), i.e. lower than 9.3 ± 10.3 kPa [43] and 16.5 ± 4.7 kPa [48] in healthy humans. However, the reduction of end-diastolic LV myofibre stress in PPCM through LVAD support did not reach values for healthy humans of 0.3 ± 1.4 kPa [48] and 2.2 ± 0.6 kPa [43].

The LVAD reduced LV and RV myofibre stresses to lower levels in PPCM than in heart failure reported in a previous study [22]. The reduction in end-systolic LV myofibre stress by LVAD support was larger for PPCM (-72.0%) than for chronic heart failure (-6.7%) [22] despite similar myofibre stress without LVAD, i.e. 30.2 ± 31.5 kPa and 35.7 ± 5.6 kPa [22].

The chronic heart failure in Sack [22] was due to ischemia and this could explain the lower myofiber stress reduction compared to PPCM which is cardiac muscle pathology whose primary insult (pregnancy) does not persist like in other heart failure conditions due to ischemia (part of the cardiac tissue is dead) or genetic cardiomyopathies. A study by Loyaga-Rendon [12] reported a higher survival rate for PPCM patients (83%) than non-ischemic cardiomyopathy (65%) and ischemic cardiomyopathy patients (64%), two years after receiving mechanical circulatory support. The LVAD (n = 1123) was the most used device compared to the Bi-ventricular assist device (n = 121) and total artificial heart (n = 14) [12]. Mechanical circulatory support is given to severe acute PPCM patients who do not respond

to drug therapy alone [10] but the reasons for the higher device recovery and survival rates in PPCM than other forms of heart failure are not yet well understood and need further investigation.

Long-term use of LVAD is associated with adverse events, including right ventricular failure (Hitzeroth et al. 2020, Rich et al. 2017). The current study predicted higher myofibre stress in the RV than the LV at each LVAD speed, yet myofibre stress was lower in the RV than the LV without LVAD (Table 6). Due to the interdependence between LV and RV, the effective unloading of the LV by the LVAD is reported to cause volume and pressure overload and elevated myofibre stress in the RV [22, 23]. Similar to a study on chronic heart failure [22], the current study with six PPCM patients with different LVEF observed ventricular interdependence but not worsening RV failure due to LVAD support typically indicated by elevated end-diastolic RV pressure of > 15 mmHg [49, 50]. The increase in RV ejection fraction as a result of increased RV preload could indicate better RV compliance and capacity in PPCM to adapt to the additional volume from the LVAD.

4.4. Myocardial strain

Data on myofibre strains in the literature is scarce for humans but available for other species such as porcine. For PPCM, the end-systolic average myofibre strain was significantly higher in the RV than the LV, similar to findings for heart failure in porcine by Sack [32].

LV mean myofibre strain in PPCM without LVAD (end-diastole: 4.4% ± 3.3%, end-systole: -6.7% ± 3.5%) was lower than for healthy hearts at both time points (end-diastole: 9.6% ± 6.7%, end-systole: -9.8% ± 5.0%) [32]. Compared to heart failure (end-diastole: 6.9% ± 4.3%, end-systole: -5.4% ± 6.5%) [32], PPCM myofibre strain was lower at end-diastole but similar at end-systole.

LVAD support reduced myofibre strain in PPCM (Table 7) to below that for healthy subjects (at end-diastole and end-systole) and heart failure (at end-diastole but not end-systole) [32]. The end-systolic LV myofibre strain was slightly higher in PPCM with LVAD support than in heart failure [32]. The continuous unloading during diastole could have restricted the full relaxation of the LV at end-diastole and thus the lower strains. At end-systole, the LVAD could have further reduced the LV volume and enhanced contraction, resulting in the higher strain.

4.5. Limitations

The small sample size of six PPCM patients and the unequal patient numbers in the recovered (two) and not recovered (four) limited generalised conclusions about PPCM and the impact of LVAD support in PPCM. Future studies should involve larger patient numbers and equal group sizes to confirm the current results.

In the current study, the biventricular geometries truncated at the base of the ventricles did not include some anatomical structures, such as papillary muscles and atria. Future research may consider incorporating these anatomical features to advance cardiac computational models.

The lack of *in vivo* data such as ventricular pressure and myocardial strain restricted the validation of the PPCM models in this study. Nonetheless, the model calibration used has been validated [32] and produced reasonable results. This is confirmed in the current study as the PPCM myofibre stresses were similar to heart failure stresses, as may be expected, and elevated compared to myofibre stresses in the healthy heart. In the future, more PPCM models should be developed and validated using *in vivo* pressure and strain data.

The material law used in the PPCM models activates contraction at the same time everywhere in the ventricles compared to the more realistic propagation of the electrical activation from Sinoatrial node to the atrioventricular node, bundle of His and Purkinje fibres. For simplicity, the heart rate for all the models was 77 beats per minute. In the future, electrophysiology and the patient's heart rate should be accounted for in the PPCM models.

The optimisation to obtain the patient-specific values of the constitutive parameters were performed using LV measurements. This could explain the high discrepancies in the *in vivo* and *in silico* RV ejection fraction in this study. Future studies should incorporate RV quantities in optimisation to obtain patient-specific models.

5. Conclusions

The current study demonstrated the potential of personalised treatment to improve partial LVAD support in PPCM patients with different disease severity in South Africa. The functional improvement was greater for PPCM patients with lower EF resulting from higher disease severity than those with higher EF and lower disease severity. The results also suggest that partial LVAD support is more beneficial for patients with PPCM than those with chronic heart failure due to ischemia. The developed patient-specific models offer a tool for further research into characterisation and treatment of PPCM. For example, identifying specific distinctive characteristics of PPCM may enable differential diagnosis of this condition, leading to more timely interventions and management. Focus of further research into LVAD support in PPCM should include patient- and disease-stage specific treatment options to guide clinical decisions and optimise personalised therapy outcomes.

Data availability

Computational models and data supporting this study are available on the University of Cape Town's institutional data repository ZivaHub under the DOI https://doi.org/10.25375/uct.26047783 as Nagawa J, Sack KL, Nchejane NJ, Motchon YD, Sirry MS, Kraus S, Davies NH, Ntusi NAB, Franz T. Software

and data for Patient-specific in silico prediction of outcomes of partial continuous-flow LVAD treatment in peripartum cardiomyopathy. ZivaHub, 2024, DOI: 10.25375/uct.26047783.

Acknowledgements

The authors thank Associate Professor Sulaiman Moosa, Head of the Division of Radiology, University of Cape Town, for helping with the data transfer during the study. We would also like to thank the Living Heart Project for providing us with support and the Abaqus license (Dassault Systèmes, Providence, USA) which enabled us to efficiently develop patient-specific models and perform simulations in this study.

Funding

This work was financially supported by the Dr. Leopold und Carmen Ellinger Stiftung (UCT Three-Way PhD Global Partnership Programme Grant DAD937134 to TF), the National Research Foundation of South Africa (IFR14011761118 to TF), the CSIR Centre for High Performance Computing (CHPC Flagship Project Grant IRMA9543 to TF), the German Academic Exchange Service and the African Institute for Mathematical Sciences (DAAD-AIMS In-Region PhD scholarship South Africa to JN). The funders had no role in study design, data collection and analysis, decision to publish, or preparation of the manuscript. Any opinion, findings, conclusions, and recommendations expressed in this publication are those of the authors, and therefore, the funders do not accept any liability.

Competing Interests

The authors declare that they have no competing interests.

Credit Author Contributions

Juliet Nagawa: Data curation, Formal analysis, Investigation, Methodology, Project administration, Software, Validation, Visualization, Writing – Original Draft Preparation, Writing – Review & Editing

Kevin L. Sack: Conceptualization, Methodology, Software, Supervision, Writing – Review & Editing

N. John Nchejane: Methodology, Writing – Review & Editing

Y. Dodzi Motchon: Methodology, Writing – Review & Editing

Mazin Sirry: Methodology, Software, Supervision, Writing – Review & Editing

Sarah Kraus: Conceptualization, Data curation, Resources, Writing – Review & Editing

Neil H. Davies: Conceptualization, Supervision, Writing – Review & Editing

Ntobeko A.B. Ntusi: Conceptualization, Data curation, Resources, Writing – Review & Editing

Thomas Franz: Conceptualization, Data curation, Funding acquisition, Methodology, Project administration, Resources, Supervision, Validation, Writing – Original Draft Preparation, Writing – Review & Editing

References

1. Agbor VN, Essouma M, Ntusi NA, Nyaga UF, Bigna JJ, Noubiap JJ. Heart failure in sub-saharan africa: A contemporaneous systematic review and meta-analysis. *International Journal of Cardiology* 2018; **257**:207-215.
2. Sliwa K, Petrie MC, Hilfiker-Kleiner D, Mebazaa A, Jackson A, Johnson MR, van der Meer P, Mbakwem A, Bauersachs J. Long-term prognosis, subsequent pregnancy, contraception and overall management of peripartum cardiomyopathy: Practical guidance paper from the heart failure association of the european society of cardiology study group on peripartum cardiomyopathy. *European Journal of Heart Failure* 2018; **20**:951-962.
3. Soma-Pillay P, Seabe J, Sliwa K. The importance of cardiovascular pathology contributing to maternal death: Confidential enquiry into maternal deaths in south africa, 2011-2013: Cardiovascular topics. *Cardiovascular Journal of Africa* 2016; **27**:60-65.
4. McNamara DM, Elkayam U, Alharethi R, Damp J, Hsich E, Ewald G, Modi K, Alexis JD, Ramani GV, Semigran MJ. Clinical outcomes for peripartum cardiomyopathy in north america: Results of the ipac study (investigations of pregnancy-associated cardiomyopathy). *Journal of the American College of Cardiology* 2015; **66**:905-914.
5. Renjithlal SLM, Munshi RF, Eid M, Zaalouk M, Cordeiro N, Pillai NU, Ritter N. Racial equity, use of mechanical support and outcomes in peripartum cardiomyopathy in united states. *Journal of the American College of Cardiology* 2023; **81**:2141-2141.
6. Sliwa K, van der Meer P, Viljoen C, Jackson AM, Petrie MC, Mebazaa A, Hilfiker-Kleiner D, Maggioni AP, Laroche C, Regitz-Zagrosek V. Socio-economic factors determine maternal and neonatal outcomes in women with peripartum cardiomyopathy: A study of the esc eorp ppcm registry. *International Journal of Cardiology* 2024; **398**:131596.
7. Laliberte B, Reed BN, Ather A, Devabhakthuni S, Watson K, Lardieri AB, Baker-Smith CM. Safe and effective use of pharmacologic and device therapy for peripartum cardiomyopathy. *Pharmacotherapy* 2016; **36**:955-970.
8. Viljoen C, Hoevelmann J, Sliwa K. Peripartum cardiomyopathy: Risk factors and predictors of outcome. *Current Opinion in Cardiology* 2023; **38**:223-232.
9. Hoevelmann J, Engel ME, Muller E, Hohlfeld A, Böhm M, Sliwa K, Viljoen C. A global perspective on the management and outcomes of peripartum cardiomyopathy: A systematic review and meta-analysis. *European Journal of Heart Failure* 2022; **24**:1719-1736.

10. Bauersachs J, König T, van der Meer P, Petrie MC, Hilfiker-Kleiner D, Mbakwem A, Hamdan R, Jackson AM, Forsyth P, de Boer RA. Pathophysiology, diagnosis and management of peripartum cardiomyopathy: A position statement from the heart failure association of the european society of cardiology study group on peripartum cardiomyopathy. *European Journal of Heart Failure* 2019; **21**:827-843.
11. Berliner D, Li T, Mariani S, Hamdan R, Hanke J, König T, Pfeffer TJ, Abou-Moulig V, Dogan G, Hilfiker-Kleiner D. Clinical characteristics and long-term outcomes in patients with peripartum cardiomyopathy (ppcm) receiving left ventricular assist devices (lvad). *Artificial Organs* 2023; **47**:417-424.
12. Loyaga-Rendon RY, Pamboukian SV, Tallaj JA, Acharya D, Cantor R, Starling RC, Naftel D, Kirklin J. Outcomes of patients with peripartum cardiomyopathy who received mechanical circulatory support: Data from the intermacs registry. *Circulation: Heart Failure* 2014; **7**:300-309.
13. Djordjevic I, Merkle J, Eghbalzadeh K, Sabashnikov A, Ivanov B, Gummert J, Potapov E, Schoenrath F, Meyns B, Özbaran M. The outcome of patients with peripartum cardiomyopathy and consecutive implantation of a left ventricular assist device. *Journal of Cardiac Surgery* 2021; **36**:2651-2657.
14. Ellis JE, Ansari AA, Fett JD, Carraway RD, Randall HW, Mosunjac MI, Sundstrom JB. Inhibition of progenitor dendritic cell maturation by plasma from patients with peripartum cardiomyopathy: Role in pregnancy-associated heart disease. *Journal of immunology research* 2005; **12**:265-273.
15. Desai D, Moodley J, Naidoo D. Peripartum cardiomyopathy: Experiences at king edward viii hospital, durban, south africa and a review of the literature. *Tropical Doctor* 1995; **25**:118-123.
16. Kolte D, Khera S, Aronow WS, Palaniswamy C, Mujib M, Ahn C, Jain D, Gass A, Ahmed A, Panza JA. Temporal trends in incidence and outcomes of peripartum cardiomyopathy in the united states: A nationwide population-based study. *Journal of the American Heart Association* 2014; **3**:e001056.
17. Haghikia A, Podewski E, Libhaber E, Labidi S, Fischer D, Roentgen P, Tsikas D, Jordan J, Lichtinghagen R, Von Kaisenberg C. Phenotyping and outcome on contemporary management in a german cohort of patients with peripartum cardiomyopathy. *Basic Research in Cardiology* 2013; **108**:1-13.
18. Kamiya CA, Kitakaze M, Ishibashi-Ueda H, Nakatani S, Murohara T, Tomoike H, Ikeda T. Different characteristics of peripartum cardiomyopathy between patients complicated with and without hypertensive disorders. *Circulation Journal* 2011; **75**:1975-1981.
19. Kraus SM, Samuels P, Jermy S, Laing N, Van der Wall M, September U, Ntsekhe M, Chin A, Moosa S, Sliwa K. Clinical and cardiovascular magnetic resonance profile of cardiomyopathy

patients from south africa: Pilot of the imhotep study. *International Journal of Cardiology* 2024; **399**.

20. Dokainish H, Teo K, Zhu J, Roy A, AlHabib KF, ElSayed A, Palileo-Villaneuva L, Lopez-Jaramillo P, Karaye K, Yusoff K, Orlandini A, Sliwa K, Mondo C, Lanas F, Prabhakaran D, Badr A, Elmaghawry M, Damasceno A, Tibazarwa K, Belley-Cote E, Balasubramanian K, Islam S, Yacoub MH, Huffman MD, Harkness K, Grinvalds A, McKelvie R, Bangdiwala SI, Yusuf S, Campos R, Chacón C, Cursack G, Diez F, Escobar C, Garcia C, Vilamajo OG, Hominal M, Ingaramo A, Kucharczuk G, Pelliza M, Rojas A, Villani A, Zapata G, Bourke P, Lanas F, Nahuelpan L, Olivares C, Riquelme R, Ai F, Bai X, Chen X, Chen Y, Gao M, Ge C, He Y, Huang W, Jiang H, Liang T, Liang X, Liao Y, Liu S, Luo Y, Lu L, Qin S, Tan G, Tan H, Wang T, Wang X, Wei F, Xiao F, Zhang B, Zheng T, Mendoza JLA, Anaya MB, Gomez E, de Salazar DIM, Quiroz F, Rodríguez MJ, Sotomayor MS, Navas AT, León MB, Montalvo LAF, Jaramillo ML, Patiño EP, Perugachi C, Trujillo Cruz F, Elmaghawry M, Wagdy K, Bhardwaj AK, Chaturvedi V, Gokhale GK, Gupta R, Honnutagi R, Joshi P, Ladhani S, Negi PC, Roy A, Reddy N, Abdullah A, Hassan MRA, Balasinga M, Kasim S, Tan WY, Yusoff K, Damasceno A, Banze R, Calua E, Novela C, Chemane J, Akintunde AA, Ansa V, Gbadamosi H, Karaye KM, Mbakwem A, Mohammed S, Nwafor E, Ojji D, Olunuga T, Sa'idu BOH, Umuerri E, Alcaraz J, Palileo-Villanueva L, Palomares E, Timonera MR, Badr A, Alghamdi S, Alhabib K, Almasood A, Alsaif S, Elasfar A, Ghabashi A, Mimish L, Bester F, Kelbe D, Klug E, Sliwa K, Tibarzawa K, Abdalla OE, Dimitri ME, Mustafa H, Osman O, Saad A, Mondo C. Global mortality variations in patients with heart failure: Results from the international congestive heart failure (inter-chf) prospective cohort study. *The Lancet global health* 2017; **5**:e665-e672.

21. Hitzeroth J, Mpe M, Klug E, Ranjith N, Sliwa K, Steingo L, Lachman L, Tsabedze N, Ntusi N. 2020 heart failure society of south africa perspective on the 2016 european society of cardiology chronic heart failure guidelines. *South African Medical Journal* 2020; **110**.

22. Sack KL, Dabiri Y, Franz T, Solomon SD, Burkhoff D, Guccione JM. Investigating the role of interventricular interdependence in development of right heart dysfunction during lvad support: A patient-specific methods-based approach. *Frontiers in Physiology* 2018; **9**:520.

23. Scardulla F, Agnese V, Romano G, Di Gesaro G, Sciacca S, Bellavia D, Clemenza F, Pilato M, Pasta S. Modeling right ventricle failure after continuous flow left ventricular assist device: A biventricular finite-element and lumped-parameter analysis. *Cardiovascular Engineering and Technology* 2018:1-11.

24. Sack KL, Aliotta E, Choy JS, Ennis DB, Davies NH, Franz T, Kassab GS, Guccione JM. Intra-myocardial alginate hydrogel injection acts as a left ventricular mid-wall constraint in swine. *Acta Biomaterialia* 2020; **111**:170-180.

25. Motchon YD, Sack KL, Sirry MS, Kruger M, Pauwels E, Van Loo D, De Muynck A, Van Hoorebeke L, Davies NH, Franz T. Effect of biomaterial stiffness on cardiac mechanics in a biventricular infarcted rat heart model with microstructural representation of in situ intramyocardial injectate. *International Journal for Numerical Methods in Biomedical Engineering* 2023; **39**:e3693.

26. Wong P, Wisneski AD, Sandhu A, Wang Z, Mahadevan VS, Nguyen TC, Guccione JM. Looking towards the future: Patient-specific computational modeling to optimize outcomes for transcatheter mitral valve repair. *Frontiers in Cardiovascular Medicine* 2023; **10**:688.

27. Lee LC, Wenk JF, Zhong L, Klepach D, Zhang Z, Ge L, Ratcliffe MB, Zohdi TI, Hsu E, Navia JL, Kassab GS, Guccione JM. Analysis of patient-specific surgical ventricular restoration: Importance of an ellipsoidal left ventricular geometry for diastolic and systolic function. *Journal of Applied Physiology* 2013; **115**:136-144.

28. Sack KL, Davies NH, Guccione JM, Franz T. Personalised computational cardiology: Patient-specific modelling in cardiac mechanics and biomaterial injection therapies for myocardial infarction. *Heart Failure Reviews* 2016; **21**:815-826.

29. Sliwa K, Hilfiker-Kleiner D, Petrie MC, Mebazaa A, Pieske B, Buchmann E, Regitz-Zagrosek V, Schaufelberger M, Tavazzi L, Veldhuisen DJ. Current state of knowledge on aetiology, diagnosis, management, and therapy of peripartum cardiomyopathy: A position statement from the heart failure association of the european society of cardiology working group on peripartum cardiomyopathy. *European Journal of Heart Failure* 2010; **12**:767-778.

30. Lang RM, Badano LP, Mor-Avi V, Afilalo J, Armstrong A, Ernande L, Flachskampf FA, Foster E, Goldstein SA, Kuznetsova T. Recommendations for cardiac chamber quantification by echocardiography in adults: An update from the american society of echocardiography and the european association of cardiovascular imaging. *European Heart Journal Cardiovascular Imaging* 2015; **16**:233-271.

31. Lang RM, Bierig M, Devereux RB, Flachskampf FA, Foster E, Pellikka PA, Picard MH, Roman MJ, Seward J, Shanewise JS. Recommendations for chamber quantification: A report from the american society of echocardiography's guidelines and standards committee and the chamber quantification writing group, developed in conjunction with the european association of echocardiography, a branch of the european society of cardiology. *Journal of the American Society of Echocardiography* 2005; **18**:1440-1463.

32. Sack KL, Aliotta E, Ennis DB, Choy JS, Kassab GS, Guccione JM, Franz T. Construction and validation of subject-specific biventricular finite-element models of healthy and failing swine hearts from high-resolution dt-mri. *Frontiers in Physiology* 2018; **9**.

33. Holzapfel GA, Ogden RW. Constitutive modelling of passive myocardium: A structurally based framework for material characterization. *Philosophical Transactions of the Royal Society of London, Series A: Mathematical and Physical Sciences* 2009; **367**:3445-3475.

34. Dokos S, Smaill BH, Young AA, LeGrice IJ. Shear properties of passive ventricular myocardium. *American Journal of Physiology: Heart and Circulatory Physiology* 2002; **283**:H2650-H2659.

35. Guccione J, Waldman L, McCulloch A. Mechanics of active contraction in cardiac muscle: Part ii—cylindrical models of the systolic left ventricle. *Journal of Biomechanical Engineering* 1993; **115**:82-90.

36. Sack KL, Baillargeon B, Acevedo-Bolton G, Genet M, Rebelo N, Kuhl E, Klein L, Weiselthaler GM, Burkhoff D, Franz T. Partial lvad restores ventricular outputs and normalizes lv but not rv stress distributions in the acutely failing heart in silico. *International Journal of Artificial Organs* 2016; **39**:421.

37. Klotz S, Hay I, Dickstein ML, Yi G-H, Wang J, Maurer MS, Kass DA, Burkhoff D. Single-beat estimation of end-diastolic pressure-volume relationship: A novel method with potential for noninvasive application. *American Journal of Physiology: Heart and Circulatory Physiology* 2006; **291**:H403-H412.

38. Nagueh SF, Middleton KJ, Kopelen HA, Zoghbi WA, Quiñones MA. Doppler tissue imaging: A noninvasive technique for evaluation of left ventricular relaxation and estimation of filling pressures. *Journal of the American College of Cardiology* 1997; **30**:1527-1533.

39. Sommer G, Schriefl AJ, Andrä M, Sacherer M, Viertler C, Wolinski H, Holzapfel GA. Biomechanical properties and microstructure of human ventricular myocardium. *Acta Biomaterialia* 2015; **24**:172-192.

40. Carreras F, Garcia-Barnes J, Gil D, Pujadas S, Li CH, Suarez-Arias R, Leta R, Alomar X, Ballester M, Pons-Llado G. Left ventricular torsion and longitudinal shortening: Two fundamental components of myocardial mechanics assessed by tagged cine-mri in normal subjects. *The International Journal of Cardiovascular Imaging* 2012; **28**:273-284.

41. Anonymous. *Abaqus theory guide*. Version 6.14. 2014, Providence: Dassault Systèmes SIMULIA Corp.

42. Dabiri Y, Sack KL, Shaul S, Sengupta PP, Guccione J. Relationship of transmural variations in myofiber contractility to left ventricular ejection fraction: Implications for modeling heart failure phenotype with preserved ejection fraction. *Frontiers in Physiology* 2018; **9**:1003.

43. Genet M, Lee LC, Nguyen R, Haraldsson H, Acevedo-Bolton G, Zhang Z, Ge L, Ordovas K, Kozerke S, Guccione JM. Distribution of normal human left ventricular myofiber stress at end diastole and end systole: A target for in silico design of heart failure treatments. *Journal of Applied Physiology* 2014; **117**:142-152.

44. Dabiri Y, Sack KL, Rebelo N, Wang P, Wang Y, Choy JS, Kassab GS, Guccione JM. Method for calibration of left ventricle material properties using three-dimensional echocardiography endocardial strains. *Journal of Biomechanical Engineering* 2019; **141**.

45. Guglin M, Zucker MJ, Borlaug BA, Breen E, Cleveland J, Johnson MR, Panjrath GS, Patel JK, Starling RC, Bozkurt B. Evaluation for heart transplantation and lvad implantation: Jacc council perspectives. *Journal of the American College of Cardiology* 2020; **75**:1471-1487.

46. Rusinaru D, Bohbot Y, Djelaili F, Delpierre Q, Altes A, Serbout S, Kubala M, Maréchaux S, Tribouilloy C. Normative reference values of cardiac output by pulsed-wave doppler echocardiography in adults. *The American journal of cardiology* 2021; **140**:128-133.

47. Kosaraju A, Goyal A, Grigorova Y, Makaryus AN. Left ventricular ejection fraction. 2017.

48. Wisneski AD, Wang Y, Deuse T, Hill AC, Pasta S, Sack KL, Yao J, Guccione JM. Impact of aortic stenosis on myofiber stress: Translational application of left ventricle-aortic coupling simulation. *Frontiers in Physiology* 2020; **11**:574211.

49. Atluri P, Goldstone AB, Fairman AS, MacArthur JW, Shudo Y, Cohen JE, Acker AL, Hiesinger W, Howard JL, Acker MA, Woo YJ. Predicting right ventricular failure in the modern, continuous flow left ventricular assist device era. *The Annals of Thoracic Surgery* 2013; **96**:857-864.

50. Konstam MA, Kiernan MS, Bernstein D, Bozkurt B, Jacob M, Kapur NK, Kociol RD, Lewis EF, Mehra MR, Pagani FD. Evaluation and management of right-sided heart failure: A scientific statement from the american heart association. *Circulation* 2018; **137**:e578-e622.